



Modeling ultrasonic metafluids: The significance of discrete oscillatorsAljaž Draškovič-Bračun , Tilen Potisk, and Daniel Svenšek **Laboratory of Molecular Modeling, National Institute of Chemistry, SI-1001 Ljubljana, Slovenia
and Department of Physics, Faculty of Mathematics and Physics, University of Ljubljana, SI-1000 Ljubljana, Slovenia*

(Received 8 May 2023; accepted 11 December 2023; published 5 January 2024)

Significant changes in the acoustic response of a fluid can be induced by the suspension of tiny, subwavelength-size discrete micro-oscillators in the fluid. We investigate how the topological properties of these oscillators, such as the mass distribution and connectivity of the oscillator parts, influence the effective dynamic density and compressibility of the fluid in which they are embedded. We demonstrate a superior, metamaterial-like response of the suspension when using micro-oscillators with a high density of low-frequency modes. Such low-frequency modes occur in loosely connected microstructures and make the system much more experimentally feasible due to the larger ultrasonic attenuation length at these frequencies. In addition, the absence of need for an intricately designed structure brings experimental implementation within reach.

DOI: [10.1103/PhysRevE.109.014604](https://doi.org/10.1103/PhysRevE.109.014604)**I. INTRODUCTION**

In metamaterials the interaction between waves and matter leads to unusual wave-propagating properties of the medium, which can be used in a wide array of applications: from electromagnetic absorbers [1] and cloaking devices [2] to designing perfect lenses, capable of beating the diffraction limit in subwavelength imaging [3]. In acoustic metamaterials, the parameters that determine sound propagation, i.e., the effective compressibility χ and density ρ of the wave-carrying medium, can become simultaneously negative in certain frequency windows due to resonance effects of subwavelength inclusions [4,5]. Metafluids are a special class of acoustic metamaterials, in which the inclusions are suspended in a host fluid. In existing practical realizations, the inclusions acting as micro-oscillators are typically symmetrically shaped or periodically arranged to achieve negative χ and ρ [4–17]. In such systems, monopolar resonances (breathing modes) affecting the compressibility of the system can be achieved relatively easily by the inclusion of bubble-like or vesicle-like objects [6–10,18–21]. Such hollow (gas-filled) objects are highly compressible and, together with the effective mass load of the surrounding fluid, produce resonances at ultrasonic frequencies despite their small size. Conversely, a region of the host fluid exhibits resonance—a standing wave—only on the wavelength scale.

To affect the apparent density of the suspension, the inclusions must exert a force on the fluid, and therefore the corresponding resonances must have dipolar angular symmetry. Since in metafluids there is no external structure (e.g., a skeleton in the form of a gel-like matrix) from which the inclusions could recoil, their lowest dipolar modes are rigid translations with zero frequency, which means that higher-order dipolar modes are required for any acoustic effect. Since

the inclusions are by definition much smaller than the ultrasound wavelength used, higher-order modes are difficult to achieve at the corresponding frequencies, as this requires that the speed of sound in the inclusions be much lower than that of the host fluid. Moreover, these modes are subject to a crucial requirement: to exert a net force on the host fluid, part of the active regions of these modes must be hidden from the fluid, in the sense that their coupling with the fluid is weaker.

One of the possible solutions is a heterogeneous medium containing quasihomogeneous inclusions with contrasting sound speed, such as oil droplets or highly porous spheres. While the sound speed contrast in the former is too low to achieve a full metaeffect [22], it was shown in Ref. [23] that metamaterial operation is possible with the latter. Large air cavities in the porous spheres make them highly compressible, while they maintain a relatively high mass density due to their solid skeleton, so that the resulting speed of sound inside the spheres is much lower than in the surrounding fluid.

Homogeneous objects have well-predicted acoustic modes determined by their shape alone, with resonant frequencies inversely proportional to the size and directly proportional to the speed of sound in the objects. According to multiple scattering models [24], these well-defined resonances lead to a change in the dynamic constitutive parameters ρ and χ .

While for homogeneous inclusions the response can be influenced only by adjusting the size, compressibility, and density of the objects, in our earlier work [25] we have drawn attention to a possible alternative approach. We introduced a model of ultrasonic metafluids in the form of suspensions of disordered, generally irregularly shaped discrete microscopic oscillators [Fig. 1(left)] coupled to the embedding fluid via a triangulated surface of the oscillator. Possible candidates for practical implementation range from the largest macromolecular structures to artificial, microfabricated (e.g., microprinted) objects. Such discrete oscillating structures have special properties that distinguish them from simpler continuum objects. The main interest lies in their

*daniel.svenssek@fmf.uni-lj.si

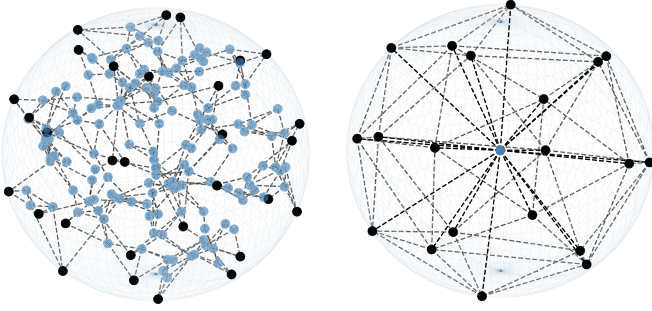


FIG. 1. Left: Example of a general discrete micro-oscillator model with internal point masses (blue), point masses defining a spheroidal surface (black), and network of bonds (dashed). Right: Simplified prototype micro-oscillator consisting of a quasispherical distribution of 20 surface points and an additional point in the center, with bonds between closest neighbors on the surface and between each surface point and the central point. In both cases, the points defining the spheroidal surface are evenly distributed at $r = r_0$ by solving the Thomson problem. Throughout this work, r_0 is set to $3 \mu\text{m}$, making the resonator much smaller than the ultrasound wavelength at the resulting frequencies.

unpredictability with respect to possible anomalous resonance effects—resonances of complex discrete structures are even qualitatively unpredictable because they depend on various structural properties such as the mass distribution and, in particular, the coordination number of important connections between particles that define the effective topology of the oscillator network.

In Ref. [25] we formulated the detailed operating principle of such a metafluid model, gave explicit formulas for its effective dynamic moduli in terms of the modal structure of the micro-oscillators, and discussed basic practical issues of performance optimization in terms of their size and density relative to the density of the embedding fluid. In Sec. II we briefly summarize the key constituents and results of this metafluid model. In Sec. III we take a simple step towards inhomogeneous inclusions and investigate the operation of micro-oscillators with different ratios of surface and core masses. In Sec. IV we focus on resonances with anomalously low frequencies, “floppy” modes, which are the main advantage of discrete oscillators from an acoustic point of view.

II. MODEL: METAFUID WITH DISCRETE OSCILLATORS

A. Effective acoustic parameters

Due to the oscillation of the inclusions excited by the sound field, the density and compressibility of the suspension as experienced by the sound wave become frequency dependent. Although, in principle, even a single inclusion changes the properties of the material (the effect does not arise from the interaction between the inclusions), it is necessary by construction for an effective metamedium that many of these structures are distributed in the liquid. For low concentrations of micro-oscillators (dilute limit) and long wavelengths relative to the size of the micro-oscillators as well as to the mean distance between them (metamaterial limit), the

effective macroscopic density $\rho^{\text{eff}}(\omega)$ and compressibility $\chi^{\text{eff}}(\omega)$ of such a metafluid at (angular) frequency ω can be briefly written as [25]

$$\rho^{\text{eff}}(\omega) \equiv \rho_0 + \rho' = \rho_0 + \phi_V(\rho - \rho_0) + \phi_V \rho \frac{\bar{x}(\omega)}{a_0}, \quad (1)$$

$$\chi^{\text{eff}}(\omega) \equiv \chi_0 + \chi' = \chi_0 + \phi_V \frac{1}{V_1} \frac{Q_1}{i\omega p}, \quad (2)$$

where ρ_0 and χ_0 are the density and compressibility of the host fluid, ρ the mean mass density of the oscillators with volumes V_1 , and ϕ_V their volume fraction that does not change with time. While the density ρ is an important factor to consider in practical implementation due to the possible sedimentation or floatation of the micro-oscillators, in this work we have neglected the effects of gravity and set $\rho = 2\rho_0$. The impact of ρ on the metamaterial-like response has been analyzed in our previous work [25]. For optimal metamaterial performance it was found that ρ should be similar to the density of the fluid. Therefore, in principle, one can design or select inclusions whose density is equal to that of the fluid and prevent sedimentation or floatation issues. In Eq. (1) the first two terms reflect a simple compositional average, while the last term comes from the dynamic influence of the oscillators: $\bar{x}(\omega)$ is the displacement of the center of mass (CM) of the oscillator in the reference frame of the acoustic velocity, i.e., relative to the long-wavelength acoustic oscillation of the host fluid, due to the excitation by the sound wave with the displacement amplitude a_0 . The dynamic compressibility χ' in Eq. (2) results from the breathing of the oscillators, i.e., from the volume flux Q_1 of the oscillator excited by the sound pressure p . Since \bar{x} and Q_1 are proportional to the excitation amplitudes a_0 and p , respectively, the excitation does not appear in Eqs. (1) and (2), and ρ^{eff} and χ^{eff} depend only on the frequency response and surface geometry of the micro-oscillator.

In Ref. [25] we described the dynamics of the micro-oscillator by its damped fluid-coupled modes and obtained \bar{x} and Q_1 as sums of modal contributions,

$$\bar{x} = \frac{1}{\sum_j m_j} \left\langle \sum_i \sum_j c_i(a_0) m_j \mathbf{x}_j^i \right\rangle = \frac{\bar{x}}{a_0} \mathbf{a}_0, \quad (3)$$

$$Q_1 = -i\omega \sum_i c_i(a_0) \sum_{\Delta^k} \frac{1}{3} \sum_{j \in \Delta^k} S^k \hat{\mathbf{n}}^k \cdot \mathbf{x}_j^i. \quad (4)$$

Here \mathbf{x}_j^i are the i th mode three-dimensional displacement vectors of the point masses m_j of the micro-oscillator and $c_i(a_0)$ are the acoustically excited amplitudes of the modes. Due to random orientations of the micro-oscillators and the resulting isotropic symmetry of the “average” oscillator provided by orientational averaging $\langle \cdot \rangle$ in Eq. (3), \bar{x} lies in the direction \mathbf{a}_0/a_0 of acoustic polarization. In Eq. (4) the volume flux is given by the deformation of the effective, triangulated surface of the oscillator, where the vertices of the triangles are the surface mass points j with corresponding displacements \mathbf{x}_j^i ; the summation Δ^k is over the surface triangles with unit normals $\hat{\mathbf{n}}^k$ and areas S^k .

B. Fluid-coupled modes

The normal modes \mathbf{x}^i and resonance frequencies ω_i of the micro-oscillator coupled to the embedding fluid are solutions

of [25]

$$\mathbf{V}\mathbf{x}^i = \omega_i^2 \mathbf{T}\mathbf{x}^i, \quad (5)$$

where \mathbf{V} is the matrix of harmonic inter-particle ‘‘spring constants,’’ which will be discussed in the next sections, and \mathbf{T} is the kinetic matrix discussed below. For an oscillator consisting of N mass points j , $\mathbf{x}^i = \{\mathbf{x}_j^i\}$ is a ‘‘supervector’’ with size $3N$ of the individual displacement vectors.

In a free oscillator, the kinetic matrix \mathbf{T} is a diagonal matrix of the particle masses m_j . However, since the oscillator in our model is coupled and must accelerate the fluid surrounding it, assuming potential flow in the fluid, it experiences an additional mass load that is reflected in a full kinetic matrix.¹ We can split it into $\mathbf{T} = \mathbf{M} + \mathbf{A}$, where $\mathbf{M} = \text{diag}(m_1, \dots, m_N)$ is diagonal, while \mathbf{A} is symmetric by construction [25] and contains contributions due to the coupling. The diagonal elements of \mathbf{A} represent additional effective hydrodynamic masses of the particles, while the off-diagonal elements are due to the hydrodynamic interactions between the parts of the micro-oscillator.

Since the matrices \mathbf{V} and \mathbf{T} are symmetric, the orthogonality condition $\mathbf{x}^j \mathbf{T} \mathbf{x}^i = 0$ holds for $\omega_j^2 \neq \omega_i^2$. The excitation amplitudes c_i required in Eqs. (3) and (4) are determined by projecting the excitation forces exerted on the oscillator particles onto the modes and are given by [25]

$$c_i(\omega) = \frac{1}{\omega_i^2 - \omega^2} \frac{\langle \mathbf{x}^i | (\mathbf{F} + \omega^2 \mathbf{M} \mathbf{a}^0) \rangle}{\langle \mathbf{x}^i | \mathbf{T} | \mathbf{x}^i \rangle}, \quad (6)$$

where \mathbf{F} is the acoustic pressure force on the surface particles and $\omega^2 \mathbf{M} \mathbf{a}^0$ is the fictitious (inertial) force in the oscillating reference frame acting on all particles; \mathbf{a}^0 is the supervector of rigid translation corresponding to acoustic oscillation with amplitude \mathbf{a}_0 . Damping is taken into account by adding an imaginary part to the eigenfrequencies, $\omega_i' = \omega_i - i\beta_i$. The damping coefficient β_i of a mode can be estimated by perturbation calculation of the viscous dissipation in the fluid flow coupled to the mode [25]. It is independent of ω_i and decreases approximately inversely proportional with the square of the micro-oscillator size. Treating viscosity as a perturbation is possible under the condition that inertial forces [described by the time derivative term in the Navier-Stokes equation (NSE)] dominate over the viscous ones. This is true when the size of the inclusions is sufficiently large compared to the penetration length of oscillatory shear, which depends on the corresponding excitation frequencies [25]. However, despite including viscosity only as a perturbation, the Reynolds number is still small, as in the case of any well-defined propagating wave.

C. Oscillator model and interparticle potential

The bonds between the oscillator particles are modeled by quadratic pair potentials U_{ij} that depend on the distance between the particles,

$$U_{ij} = \frac{1}{2} k_{ij} (|\mathbf{R}_i + \mathbf{x}_i - \mathbf{R}_j - \mathbf{x}_j| - |\mathbf{R}_i - \mathbf{R}_j|)^2, \quad (7)$$

¹If the assumption of potential (irrotational incompressible) fluid flow is relaxed and the flow is compressible and able to describe outgoing waves, there is an additional radiation load besides the mass load and \mathbf{T} is complex.

where \mathbf{R}_i are the equilibrium positions of the particles, \mathbf{x}_i their fluctuations, and k_{ij} the bond constants. In elastic network models of proteins [26–28], this potential is known as the anisotropic network model (ANM). The harmonic approximation matrix \mathbf{V} is then obtained from the total potential $U = \sum_{i<j} U_{ij}$ as

$$V_{kl} = \frac{\partial^2 U}{\partial x_k \partial x_l}, \quad (8)$$

where the derivatives are with respect to the components of the particle displacement supervector.

To demonstrate the basic metamaterial function of our micro-oscillator suspension model, we started in Ref. [25] with the simplest possible micro-oscillator prototype [Fig. 1(right)], which we will also use here in Sec. III. It consists of a spherical distribution of particles and an additional particle in the center that is not exposed to the surrounding fluid. In this simple prototype, the inner particle represents the mass of the entire internal structure. In Sec. IV, we will turn to micro-oscillators with many more particles and full network complexity.

III. MASSIVE SHELL VS MASSIVE CORE

A first step beyond homogeneous inclusion to a micro-oscillator with a somewhat richer internal structure can be made with our simple prototype of Fig. 1(right) and changing the ratio ξ between the total surface mass and the internal mass. To observe the effects on ρ' , we choose equal interactions between each surface particle and the central particle and make the interactions between the surface particles negligible. This clean choice leads to only one type of significant dipolar modes, namely, the three modes with roughly the same frequency where the central part and the surface move in opposite directions, resulting in a single resonance peak in $\rho'(\omega)$. Additionally for each ξ , we adjust the spring constants so that the frequency of the dipolar mode remains approximately constant.

The frequency response of ρ' for different values of ξ is shown in Fig. 2. The momentum transfer to the fluid, which is the cause of the change in the effective density, depends directly only on the motion of the surface, but not on its mass. For large ξ , the motion of the heavy shell in the dipolar mode is small compared to that of the light mass in the center. Therefore, the contribution to ρ' is significant only in the immediate vicinity of the resonance, where the amplitude is sufficiently large. As the shell becomes lighter, its amplitude increases while the central mass comes more and more to rest. Because of the greater motion of the shell, the momentum transfer to the fluid is larger, but the damping is also larger. However, because of the larger momentum transfer, the ρ' curve does not fall entirely below the curve for higher ξ , as it does for the real part of the resonance curve of a simple oscillator when the damping is increased. Therefore, the broadening of the ρ' curve as ξ decreases results in a useful increase in operating bandwidth. It can be concluded that optimal values for ξ are not far from 1, so that the $\rho'(\omega)$ curve is not extremely narrow, while the amplitude is still large.

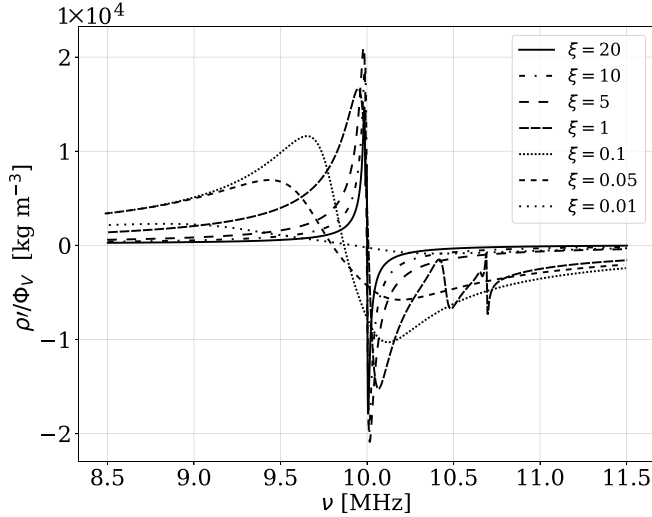


FIG. 2. Frequency dependence of the dynamic density per volume concentration ρ'/ϕ_ν at different ratios ξ of shell and core mass of the simple micro-oscillator of Fig. 1(right). Three eigenmodes with almost identical eigenfrequencies are contributing to the resonance curve. In the case of $\xi = 1$ two smaller peaks are resulting from the splitting of these resonances.

IV. SIGNIFICANCE OF “FLOPPY MODES”

For discrete objects, one of the most important aspects is the distribution of connections between the different parts of the system. Two schematic examples are shown in Fig. 3, where the connections are marked by dashed lines. The peculiarities of connectivity lead to unexpected properties and fundamental differences from the continuum, in which the particles are fully constrained by the connections and no free directions of motion remain. For example, globular proteins characterized by the cumulative number of vibrational states $G(\omega)$ were found to behave like two-dimensional objects with respect to slow vibrations [29], i.e., $G(\omega) \propto \omega^2$, which is a signature of a reduced number of interparticle connections.

Heterogeneous objects such as proteins are of particular interest because of the possibility of low-frequency floppy

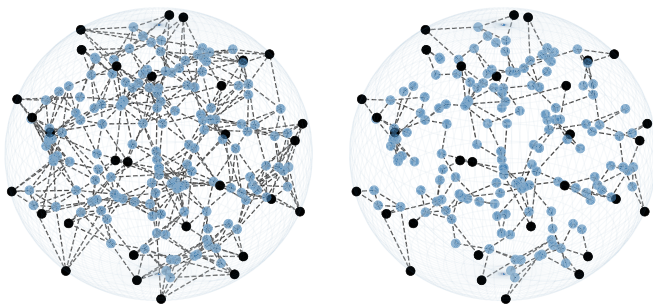


FIG. 3. Discrete oscillator models consisting of 30 surface points (black), 150 internal points (blue), and different configuration of connections (dashed). The random distribution of internal points is spatially uniform and is contained inside a sphere with radius $0.9 r_0$. The oscillators are characterized by the mean coordination number $\langle n \rangle = 6.4$, $\langle n \rangle = 2.7$, and the fraction of floppy modes $F = 0.0$, $F = 0.53$, respectively, for left and right.

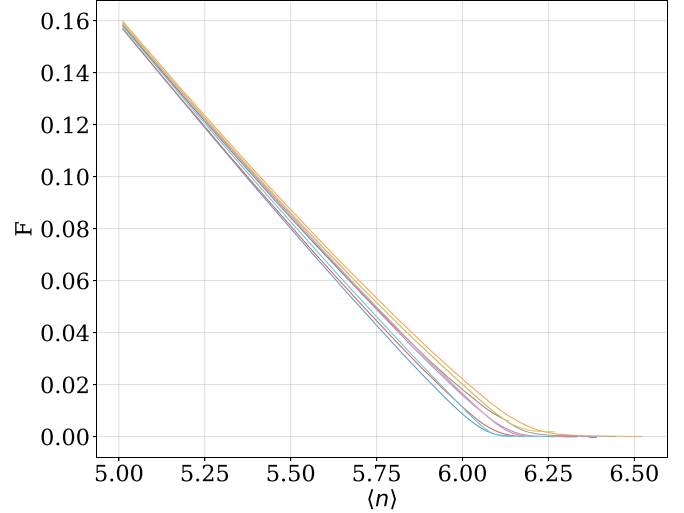


FIG. 4. Average fraction of floppy modes F vs average node degree $\langle n \rangle$ for ten different native structures, averaged over 500 random runs of removing bonds for each structure.

modes [28,30–33]. Such modes are found in structures where the absence of strong bonds between some nearby particles leads to underconstrained domains, resulting in degrees of freedom of free bond rotation whose fraction is equal to the fraction of floppy modes F (the number of floppy modes relative to the total number of eigenmodes). One of the major challenges in microscopic structures that could form the basis of an acoustic metamedium is to find relevant eigenmodes at sufficiently low frequencies where the attenuation length of ultrasound is still large enough. For macromolecular, submicron particles, this is where floppy modes come into play.

In a complex system with many particles and inter-particle connections, a model of which is shown in Fig. 3, it is not possible to predict in a simple manner, i.e., without solving the full eigenproblem, how the absence of certain connections will affect the nature of the resulting floppy modes. It is, however, possible to characterize the system statistically by the fraction of floppy modes F . The relevant structural parameter associated with F is the mean coordination number $\langle n \rangle$ (average number of bonds per atom), known in graph theory as the average node degree [34]. By simulating the gradual denaturation (bond breaking) of a number of proteins, it was observed that the change in F with the decrease in $\langle n \rangle$ followed a universal trend for all simulated proteins [30].

We observe similar behavior for our discrete oscillators (Fig. 4). These results were obtained using a structure with a spherical distribution of surface particles surrounding a random distribution of internal particles (Fig. 3). We start by connecting each particle to a sufficient number (in this case at least five) of its nearest neighbors to obtain an oscillator without floppy modes [Fig. 3(left)]. Then a desired value of $\langle n \rangle$ is reached by randomly removing bonds, for example, $\langle n \rangle = 2.7$ in Fig. 3(right). For each structure, the procedure is repeated a number of times and the average value of F vs $\langle n \rangle$ is computed (Fig. 4). The exact position of the transitional region where the floppy modes start to appear is related to the bond removal protocol. Using our random procedure, we

observe the transition region at around $\langle n \rangle = 6.2$, while in [30], where they removed bonds stepwise according to their strength and eliminated the weakest ones first, a value of $\langle n \rangle = 2.4$ was observed.

In the harmonic description [Eq. (5)] the underconstrained regions in the structure are reflected in singularities of the interaction matrix \mathbf{V} , Eq. (8). These singularities are a direct consequence of the ANM potential Eq. (7), since it depends only on the distances between the particles and does not penalize changes in the orientation of the interparticle vectors. The reduced rank of the potential matrix beyond the three translational and three rotational modes corresponds directly to the number of floppy modes in the system, which we exploit to calculate F .

Due to other potentials in the background, the frequencies of the floppy modes in a real system are of course never zero, but only “anomalously” low compared to the frequencies of the “regular” modes and can therefore extend from above 10 GHz to below the 100 MHz range suitable for the propagation of ultrasound in water. On the other hand, floppy modes with extremely low frequencies, if they exist, become useless because of their strong damping: since the damping coefficient is independent of ω_i (Sec. II B), the ratio β_i/ω_i increases and resonance is suppressed. To further lower the operating frequency, larger micro-oscillators are required.

In the numerical model, the opposite situation is usually encountered, i.e., the floppy mode frequencies are actually very close to zero and must therefore be increased to the realistically relevant range. One way to obtain a nonsingular harmonic matrix \mathbf{V} with the same configuration of connections would be to introduce an additional potential of the form

$$U_{ij}^G = \frac{1}{2}k_{ij}^G(\mathbf{x}_i - \mathbf{x}_j)^2, \quad (9)$$

also known as the Gaussian network model (GNM) [26,27,35–37], which penalizes all relative displacements equally and eliminates all free directions of motion. It turns out, however, that the addition of such a fundamentally different potential changes the shapes of all modes, which is undesirable. As pointed out in Ref. [27], GNM is the appropriate choice when evaluating deformation magnitudes or the distribution of motions of individual residues, but ANM is the only possible model when assessing the directions or mechanisms of motions. Therefore, instead of GNM, we introduce an additional weak ANM background potential between all pairs of atoms, essentially connecting them all with weak springs. Consequently, \mathbf{V} is no longer singular and frequencies of floppy modes become finite, with their magnitudes controlled by the strength of the background potential. This is a reasonable approximation of a realistic system, which retains the signature of floppy modes.

A. Influence of low-frequency modes on effective acoustic parameters

With the background potential of suitable magnitude relative to the strong bonds of the system, the floppy modes can be shifted to desirably high frequencies compared to their imaginary part, but still separate from the high-frequency nonfloppy modes. Figure 5 shows the frequency response of the effective dynamic density ρ' and compressibility χ'

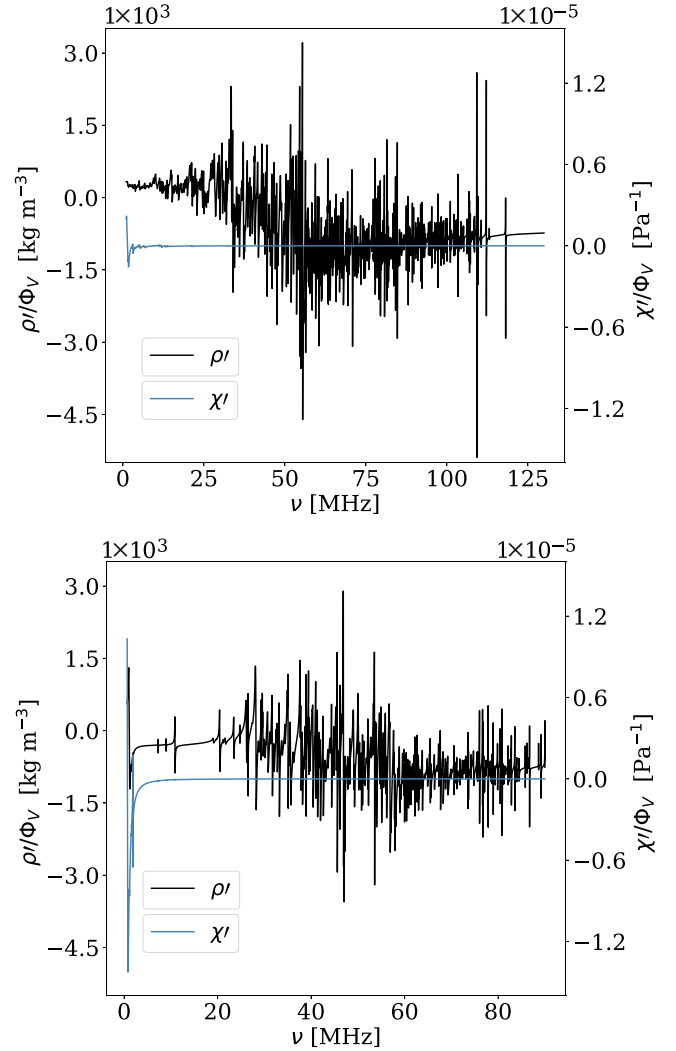


FIG. 5. Top, bottom: Frequency response of dynamic density and compressibility per volume concentration for the prototype oscillators shown in Fig. 3 left and right, respectively. The y scale is kept the same in both cases to demonstrate the impact of floppy modes.

[Eqs. (1) and (2)] for the prototype oscillators of Fig. 3. In Fig. 5(bottom) corresponding to the oscillator in Fig. 3(right) with $F = 0.53$, there are distinct peaks in the 1 MHz band for both χ' and ρ' , corresponding to floppy modes; the detailed look of this region is shown in Fig. 6(top). For the oscillator in Fig. 3(left) with $F = 0.0$, on the other hand, there are no ρ' resonances in this region, and for χ' the response is much weaker. Moreover, whereas χ' is significantly affected exclusively by low-frequency modes, interestingly enough diverse response of ρ' is present across the whole spectrum.

In general, the shapes of floppy modes can be very diverse. For example, they can have many moving parts as in Fig. 6 (middle) or only a few active sites as in Fig. 7(top). This also applies to the points on the surface that are coupled with the fluid. The corresponding solution of the velocity potential of the fluid is generally multipolar, with higher multipoles being more or less pronounced; cf. Figs. 6 and 7(bottom). Nevertheless, the volume source is completely given by the monopolar part of this solution, and the momentum transfer

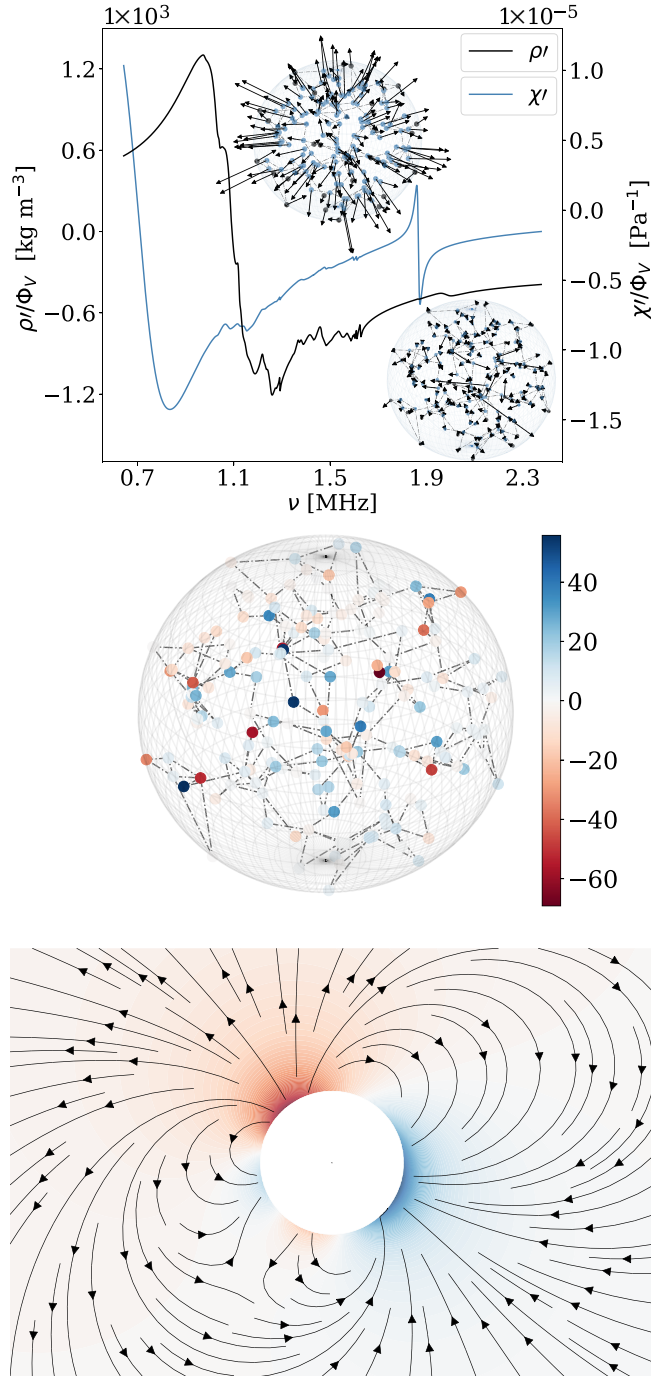


FIG. 6. Top: Detailed view of the dynamic moduli in the floppy-mode region of Fig. 5(bottom). Two modes are also shown: the upper one representing a monopole, and the lower one corresponding to the minimum of ρ'/ϕ_ν . Middle: A mode with frequency near the minimum of ρ' , yielding a predominantly dipolar velocity field. Colors represent projections of particle displacements onto the direction of the CM displacement divided by the amplitude of the CM displacement. Thus, smaller absolute values indicate efficient momentum transfer to the fluid. Bottom: Velocity potential (shading) and velocity field of the fluid corresponding to this mode, drawn in a plane containing the CM displacement.

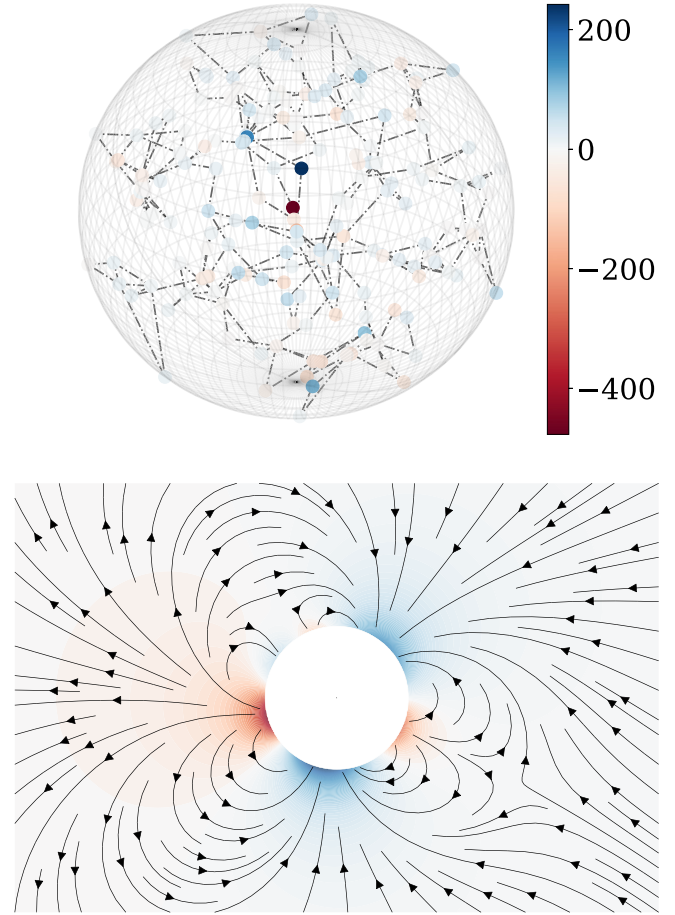


FIG. 7. Another floppy mode with frequency near the minimum of ρ' from Fig. 6 with only a few active sites (top). The corresponding velocity field and potential (bottom) contain stronger higher multipoles compared to Fig. 6, while the dipolar component is still notable.

to the fluid by its dipolar part. Thus, χ' and ρ' are determined directly from the monopolar and dipolar parts, respectively.

The momentum transferred to the fluid is, of course, opposite and equal to the momentum of the CM of the micro-oscillator. The color coding of the micro-oscillator particles in Fig. 6 (middle) and in the analogous diagrams in the following figures gives projections of the particle displacements onto the direction of the CM displacement, divided by the amplitude of the CM displacement. Thus, smaller absolute values mean that a mode displaces the fluid mass more efficiently and is a stronger source of “hidden” force exerted on the fluid. Somewhat contrary to first expectations, we observe that modes with a notable dipolar component such as that in Fig. 7 do not necessarily contain many moving particles. It is true that with only a few active particles, larger oscillation amplitudes are required to produce a hidden force effect of comparable magnitude (since only a small portion of the surface is in motion), but such modes still contribute significantly.

One must realize that the ultimate acoustic efficiency of floppy modes depends not only on the strong monopolar or dipolar contribution of a single mode, but also on the number of such modes per frequency interval. In the regions of high-frequency density of floppy modes, their acoustic effect

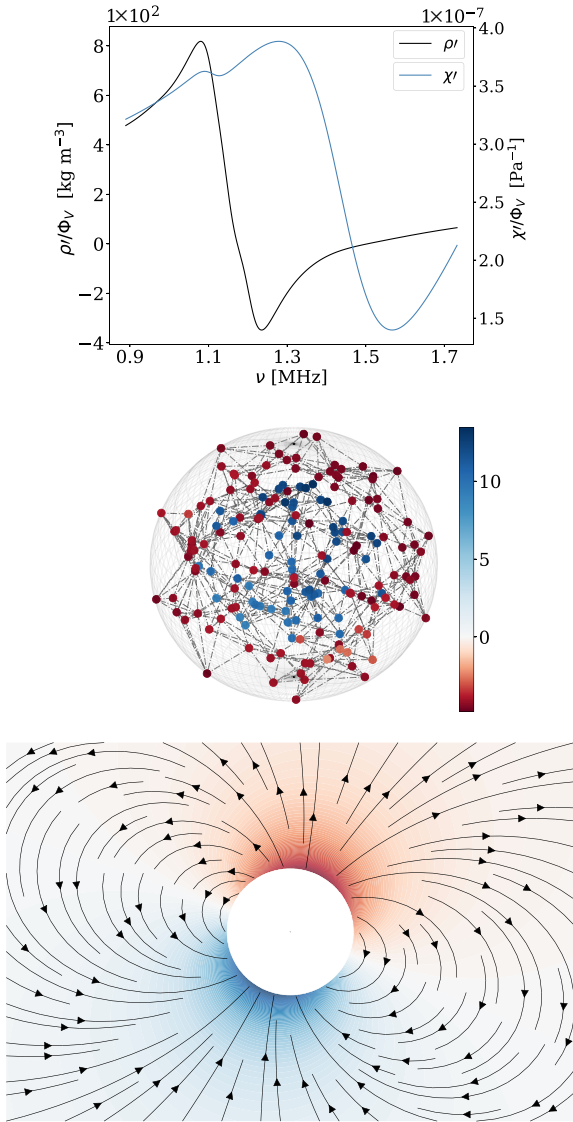


FIG. 8. Top: ρ' and χ' responses for a cluster-type micro-oscillator with 61 points in the central and 119 points in the surrounding region. Middle: One of its three collective dipolar floppy modes, color coded as explained in Fig. 6. Bottom: Corresponding velocity field and potential.

is considerably enhanced by superposition, e.g., of roughly 100 modes near the minimum of ρ' in Fig. 6.

The modes of Figs. 6 and 7 with significant dipolar components are of typical disordered, random shapes, in which even nearby particles can move in different directions, i.e., there are no regions of collective motion. In the continuum picture, this would correspond to wavelengths that are very short compared to the size of the micro-oscillator. If there were no floppy modes, such short wavelength vibrations could be found only at very high frequencies. That such irregular, highly inhomogeneous vibrations of individual sites occur at ultrasonic frequencies, have significant dipolar components, and are also efficiently excited is rather unexpected. One would perhaps rather imagine compact, massive regions within a complex structure, only loosely connected to each

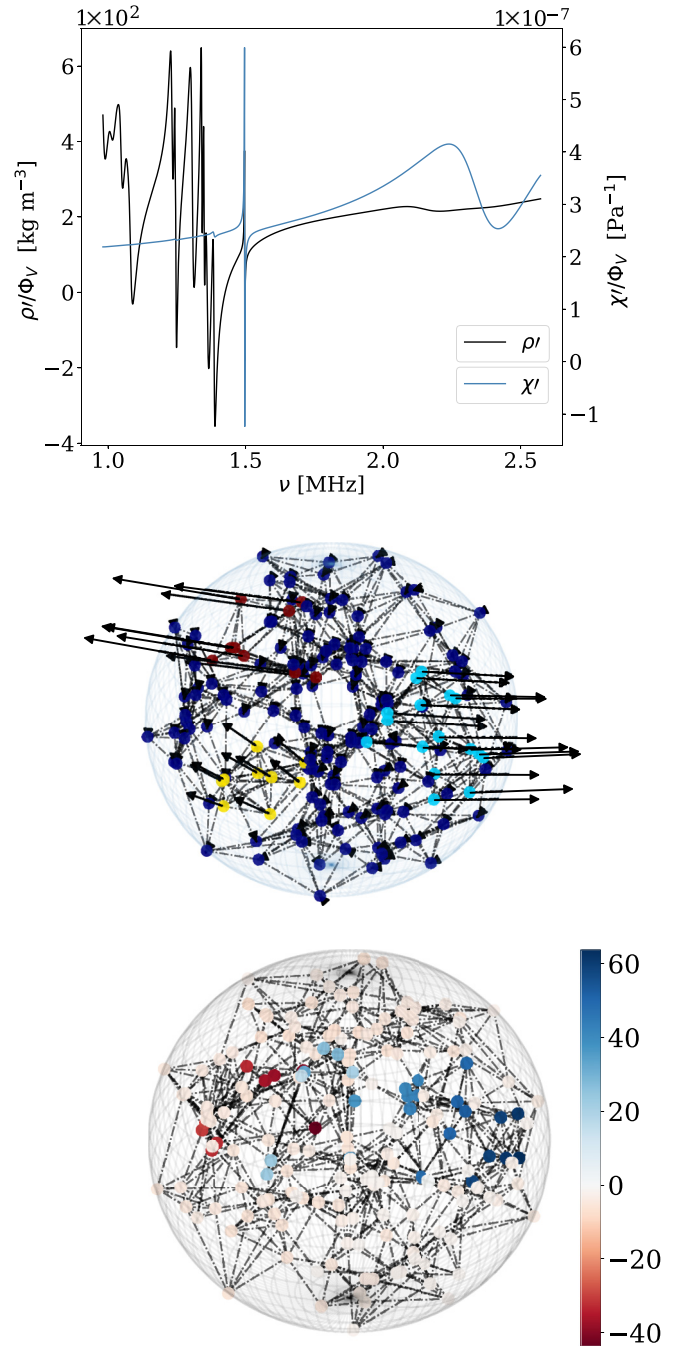


FIG. 9. ρ' and χ' responses (top) for a cluster-type micro-oscillator with four separate cluster regions marked with different colors (middle). The shape of one of its collective dipolar floppy modes is shown with arrows and (bottom) with the color coding as explained in Fig. 6; here the micro-oscillator has been rotated by an angle.

other or to the background, as more important sources of hidden force.

To study the acoustic effect of such collective modes, we model them by constructing several well intralinked regions such that they have no internal floppy modes, and using the same background potential. In this way we obtain six low-frequency modes (three translations and three rotations) for

each of these regions, which are essentially a kind of collective floppy modes whose frequencies are determined by the background potential. An example where the central region is separated from the rest of the structure is shown in Fig. 8. This collective floppy mode, responsible for the ρ' change in Fig. 8, is clearly of a different type than the floppy modes in Figs. 6 and 7. It is purely dipolar, as is the resulting velocity field in the surrounding fluid [Fig. 8(bottom)]. Given the collective vibration of the massive region, it is somewhat unexpected that the amplitude of ρ' [Fig. 8(top)] is about three times lower than in Fig. 6(top). We must note, however, that there are only three collective dipolar modes, while in the example of Fig. 6 more than 100 floppy modes with dipolar components jointly contribute to the ρ' minimum there. Figure 9 presents an oscillator with three smaller clusters spread throughout a larger one. This structure has more collective floppy modes overall than that of Fig. 8, but their effect on ρ' [Fig. 9(top)] does not add up as it does for the floppy modes of Fig. 6 because their frequencies are too far apart.

V. CONCLUSION

Suspending discrete micro-oscillators in a fluid can significantly alter its wave-propagating properties, such as the effective dynamic density or the compressibility. Using harmonic analysis of general, irregularly shaped microstructures, coupled to the fluid via their triangulated surfaces [25], we have investigated the importance of two possible topological design parameters for both the density and compressibility of the suspension: (1) the change in the ratio of the microstructure core mass to the mass of its shell and (2) the presence of low-frequency modes in loosely connected micro-oscillators.

We find that although a lower core mass compared to the mass of the shell leads to a larger decrease in the effective density of the suspension, a larger operating frequency bandwidth is obtained in the opposite case, i.e., with a lower shell mass. This is due to the larger momentum transfer from the shell, which is directly coupled to the fluid. Second, we find that the presence of low-frequency modes, which are a hallmark of loosely connected or under-constrained systems, can under certain conditions yield strong monopolar and dipolar response. In addition, we have shown that acoustic efficiency is further improved (due to superposition) in a frequency range with a high density of activated low-frequency modes. The use of micro-oscillators with such low-frequency modes has two advantages. The first is acoustic accessibility. Indeed, a serious obstacle in dealing with ultrasonic acoustic waves in water is attenuation, which increases with frequency. The floppy modes with their extremely low frequencies are therefore the most suitable candidates from this point of view. The second advantage is that the systems exhibiting floppy modes do not need to be intricately designed as is usually the case for structures in metamaterials, which makes experimental implementation a bit easier. The main problem, however, is the damping of smaller (micron- and submicron) oscillators [25] due to viscosity, especially if the eigenmodes are very slow.

ACKNOWLEDGMENTS

The authors acknowledge support through Grants No. P1-0002 and No. J1-3027 from the Slovenian Research and Innovation Agency. D.S. also acknowledges partial financial support through Grants No. J1-9149, No. N1-0195, and No. J4-3087 from the Slovenian Research Agency.

-
- [1] N. I. Landy, S. Sajuyigbe, J. J. Mock, D. R. Smith, and W. J. Padilla, Perfect metamaterial absorber, *Phys. Rev. Lett.* **100**, 207402 (2008).
 - [2] J. B. Pendry, D. Schurig, and D. R. Smith, Controlling electromagnetic fields, *Science* **312**, 1780 (2006).
 - [3] J. B. Pendry, Negative refraction makes a perfect lens, *Phys. Rev. Lett.* **85**, 3966 (2000).
 - [4] J. Li and C. T. Chan, Double-negative acoustic metamaterial, *Phys. Rev. E* **70**, 055602(R) (2004).
 - [5] Y. Ding, Z. Liu, C. Qiu, and J. Shi, Metamaterial with simultaneously negative bulk modulus and mass density, *Phys. Rev. Lett.* **99**, 093904 (2007).
 - [6] V. Leroy, A. Strybulevych, M. G. Scanlon, and J. H. Page, Transmission of ultrasound through a single layer of bubbles, *Eur. Phys. J. E* **29**, 123 (2009).
 - [7] V. Leroy, A. Strybulevych, M. Lanoy, F. Lemoult, A. Tourin, and J. H. Page, Superabsorption of acoustic waves with bubble metascreens, *Phys. Rev. B* **91**, 020301(R) (2015).
 - [8] M. Lanoy, J. H. Page, G. Lerosey, F. Lemoult, A. Tourin, and V. Leroy, Acoustic double negativity induced by position correlations within a disordered set of monopolar resonators, *Phys. Rev. B* **96**, 222011(R) (2017).
 - [9] V. Leroy, N. Chastrette, M. Thiery, O. Lombard, and A. Tourin, Acoustics of bubble arrays: Role played by the dipole response of bubbles, *Fluids* **3**, 95 (2018).
 - [10] P.-G. Luan, Bubbly water as a natural metamaterial of negative bulk-modulus, *Crystals* **9**, 457 (2019).
 - [11] H. Ammari, B. Fitzpatrick, D. Gontier, H. Lee, and H. Zhang, Minnaert resonances for acoustic waves in bubbly media, *Ann. Inst. Henri Poincaré C* **35**, 1975 (2018).
 - [12] M. Lanoy, R. Pierrat, F. Lemoult, M. Fink, V. Leroy, and A. Tourin, Subwavelength focusing in bubbly media using broadband time reversal, *Phys. Rev. B* **91**, 224202 (2015).
 - [13] L. Saviot, C. H. Netting, and D. B. Murray, Damping by bulk and shear viscosity of confined acoustic phonons for nanostructures in aqueous solution, *J. Phys. Chem. B* **111**, 7457 (2007).
 - [14] V. Galstyan, O. S. Pak, and H. A. Stone, A note on the breathing mode of an elastic sphere in Newtonian and complex fluids, *Phys. Fluids* **27**, 032001 (2015).
 - [15] Z. Boltaev, I. Safarov, and T. Razokov, Natural vibrations of spherical inhomogeneity in a viscoelastic medium, *Int. J. Sci. Technol. Res.* **9**, 3674 (2020).
 - [16] J. Mei, Z. Liu, W. Wen, and P. Sheng, Effective mass density of fluid-solid composites, *Phys. Rev. Lett.* **96**, 024301 (2006).
 - [17] Z. Liu, C. T. Chan, and P. Sheng, Analytic model of phononic crystals with local resonances, *Phys. Rev. B* **71**, 014103 (2005).
 - [18] J. R. Lindner, Microbubbles in medical imaging: Current applications and future directions, *Nat. Rev. Drug Disc.* **3**, 527 (2004).

- [19] N. Deshpande, A. Needles, and J. K. Willmann, Molecular ultrasound imaging: Current status and future directions, *Clin. Radiol.* **65**, 567 (2010).
- [20] H. Lee, H. Kim, H. Han, M. Lee, S. Lee, H. Yoo, J. H. Chang, and H. Kim, Microbubbles used for contrast enhanced ultrasound and theragnosis: A review of principles to applications, *Biomed. Eng. Lett.* **7**, 59 (2017).
- [21] D. Maresca, A. Lakshmanan, M. Abedi, A. Bar-Zion, A. Farhadi, G. J. Lu, J. O. Szablowski, D. Wu, S. Yoo, and M. G. Shapiro, Biomolecular ultrasound and sonogenetics, *Annu. Rev. Chem. Biomol. Eng.* **9**, 229 (2018).
- [22] T. Brunet, S. Raffy, B. Mascaro, J. Leng, R. Wunenburger, O. Mondain-Monval, O. Poncelet, and C. Aristégui, Sharp acoustic multipolar-resonances in highly monodisperse emulsions, *Appl. Phys. Lett.* **101**, 011913 (2012).
- [23] T. Brunet, A. Merlin, B. Mascaro, K. Zimny, J. Leng, O. Poncelet, C. Aristégui, and O. Mondain-Monval, Soft 3D acoustic metamaterial with negative index, *Nat. Mater.* **14**, 384 (2015).
- [24] P. C. Waterman and R. Truell, Multiple scattering of waves, *J. Math. Phys.* **2**, 512 (1961).
- [25] A. Draškovič-Bračun, T. Potisk, M. Praprotnik, and D. Svenšek, Suspension of discrete microscopic oscillators as a model of an ultrasonic metafluid, *Phys. Rev. B* **105**, 224317 (2022).
- [26] A. Atilgan, S. Durell, R. Jernigan, M. Demirel, O. Keskin, and I. Bahar, Anisotropy of fluctuation dynamics of proteins with an elastic network model, *Biophys. J.* **80**, 505 (2001).
- [27] A. Rader, C. Chennubhotla, L.-W. Yang, and I. Bahar, The Gaussian network model: Theory and applications, *Normal Mode Analysis: Theory and Applications to Biological and Chemical Systems*, edited by Q. Cui and I. Bahar (Chapman & Hall/CRC, Taylor & Francis Group, 2005), pp. 41–64.
- [28] S. Mahajan and Y.-H. Sanejouand, On the relationship between low-frequency normal modes and the large-scale conformational changes of proteins, *Arch. Biochem. Biophys.* **567**, 59 (2015).
- [29] D. ben-Avraham, Vibrational normal-mode spectrum of globular proteins, *Phys. Rev. B* **47**, 14559 (1993).
- [30] A. J. Rader, B. M. Hespeneide, L. A. Kuhn, and M. F. Thorpe, Protein unfolding: Rigidity lost, *Proc. Natl. Acad. Sci. USA* **99**, 3540 (2002).
- [31] M. V. Chubynsky and M. F. Thorpe, Algorithms for three-dimensional rigidity analysis and a first-order percolation transition, *Phys. Rev. E* **76**, 041135 (2007).
- [32] L. Meireles, M. Gur, A. Bakan, and I. Bahar, Pre-existing soft modes of motion uniquely defined by native contact topology facilitate ligand binding to proteins, *Protein Sci.* **20**, 1645 (2011).
- [33] M. Habibi, S. S. Plotkin, and J. Rottler, Soft vibrational modes predict breaking events during force-induced protein unfolding, *Biophys. J.* **114**, 562 (2018).
- [34] L. Di Paola, M. De Ruvo, P. Paci, D. Santoni, and A. Giuliani, Protein contact networks: An emerging paradigm in chemistry, *Chem. Rev.* **113**, 1598 (2013).
- [35] W. Zheng, A unification of the elastic network model and the Gaussian network model for optimal description of protein conformational motions and fluctuations, *Biophys. J.* **94**, 3853 (2008).
- [36] H. Na and G. Song, A natural unification of GNM and ANM and the role of inter-residue forces, *Phys. Biol.* **11**, 036002 (2014).
- [37] K. Xia, K. Opron, and G.-W. Wei, Multiscale Gaussian network model (MGNM) and multiscale anisotropic network model (MANM), *J. Chem. Phys.* **143**, 204106 (2015).